Title page

Title of the manuscript:

A coupled structural and geotechnical assessment of the effects of a landslide on an ancient monastery in Central Italy

Authors:

Marialuigia Sangirardi[a], Angelo Amorosi[b], Gianmarco de Felice[c]

[a] e-mail address: marialuigia.sangirardi@uniroma3.it
Roma Tre University
Department of Engineering.
Via Vito Volterra, 62, 00146, Rome, Italy
http://www.ingegneria.uniroma3.it/

[b] e-mail address: angelo.amorosi@uniroma1.it
'Sapienza' University of Rome
Department of Structural and Geotechnical Engineering
Via Eudossiana 18, 00184 Rome, Italy
https://web.uniroma1.it/disg/

[c] e-mail address: defelice@uniroma3.it
Roma Tre University
Department of Engineering.
Via Vito Volterra, 62, 00146, Rome, Italy
http://www.ingegneria.uniroma3.it/

Corresponding Author:

Marialuigia Sangirardi
Contacts: marialuigia.sangirardi@uniroma3.it

A coupled structural and geotechnical assessment of the effects of a landslide on an ancient monastery in Central Italy

Marialuigia Sangirardi, Angelo Amorosi and Gianmarco de Felice

Abstract

Every year landslides occur all over the world as a consequence of specific ground conditions, geomorphological, physical or man-made processes. Such phenomena, often triggered by heavy rainfalls or earthquakes, can affect buildings and infrastructures, causing economic and life losses.

This work investigates the effects of a landslide, occurred on the 26th of November 2018, on the Monastry of Santa Scolastica in Subiaco (Rome), one of the most ancient and well-preserved examples of medieval architecture in Central Italy. The evolution of the damage pattern observed on the structure is discussed and related to its different causes, aiming at evaluating if possible worsening effects should or not be ascribed to the occurred landslide or to possible future similar events. The study relies on an accurate geometrical description of both the slope and the building, made possible by advanced survey tools. Most of the analyses used to simulate the history of the events occurred to the Monastry were performed by a three-dimensional non-linear finite element model. Elastic-perfectly plastic constitutive assumptions were adopted for the soil, while the structure was modelled by a three-dimensional anisotropic elastic-perfectly plastic constitutive model, specifically conceived for masonry, accounting for block dimensions and staggering joints effects.

Finite element approach has proven to be very effective in the analysis of such a coupled interaction problem, leading to a realistic representation of the interplay between the soil displacements and their effects within the structure. The safety conditions of the structure could then be assessed, and the causes of the damage pattern identified, showing that the slope movement did not worsen the pre-existing damage conditions, which should instead be ascribed to the original soil-structure interaction phenomena occurred when an extension of the original structure had been built.

Keywords:

1. Landslides
2. Masonry
3. Finite-element modelling

1. Introduction

The understanding of the impact of natural hazards on World's architectural heritage is a felt concern in the scientific community and, to deal with this issue, interdisciplinary approaches should be adopted.

Together with earthquakes, landslides are one of the most harmful geotechnical hazards affecting constructions, economy, practicability of the infrastructures and life in the hit areas. In fact, though most of the landslides usually occur in rural areas, where they can cause significant damage to roads and railways (Puzrin et al. 2010), some of them have been reported causing severe damage to monuments. Slope movements are essentially related to the loss of equilibrium conditions stemming from either the reduction of the available soil shear strength or the increase of the mobilised shear stresses along a potential failure surface. For example, landslide may occur as a consequence of a modified groundwater regime, affecting the pore water pressure distribution in the slope and, as such, the effective stress controlling the shear strength of the soil, or can be triggered by natural or man-made hazard, inducing a transient or permanent modification of the loads acting within the slope. In some cases, the risk is increased by some predisposing factors such as land urbanization of the slope, which reduces the initial margin of safety of the system.

Some well-known examples of UNESCO Sites subjected to landslides are, to cite some, the right coast of the river Moskow (Russia), the Machu Picchu cultural heritage site (Peru) or some villages in Umbria region, like Orvieto and Rocca Ripesena (Italy) (Canuti et al., 2009).

A number of studies deal with the definition of fragility curves at the urban scale, with particular reference to slow moving landslides (Negulescu et al., 2014, Palmisano et al., 2018, Peduto et al. 2018, Del Soldato et al. 2019), while analyses at the scale of the building have also been performed for both reinforced concrete (Mavrouli et al., 2014, Parisi et al., 2015, Parisi and Sabella, 2017) or masonry structures by means of strut-and-tie models (Palmisano and Elia, 2014, 2015), finite element method (Ferlisi et al. 2019) and combined particle finite element and finite element methods (Mavrouli et al. 2017).

Italy, with reference to landslide hazard, is recognized as a very vulnerable country: 620,808 landslides have been identified on the national territory, representing around the 80% of the total number of landsides in Europe. In particular, Lazio and Umbria regions are the most affected ones (ISPRA, 2007).

The Monastery of Santa Scolastica in Subiaco is a very well-preserved example of medieval architecture and it is the most ancient Benedict's monastery in the World. It is located in a landslide prone area and, due to exceptionally heavy rainfalls, a landslide occurred on the 26th of November 2018 in the vicinity of the structure, causing fear and temporary closing of the buildings, where a

monastic community is still settled. The event can be classified as a flow-type landslide (Cruden, 1996), a *fast* phenomenon typically triggered by altered hydraulic conditions or earthquakes, that may cause large losses. Some damage had been detected in a part of the structure adjacent to the landslide, raising the question whether the landslide had caused it or, possibly, worsened a pre-existing damaged condition.

To investigate this issue, a finite element (FE) approach has been adopted, following a preliminary limit equilibrium-based back analysis of the slope failure. The complex geometry of the problem, involving an articulated ancient structure with more recent inserts and a surrounding variegated morphology of the site, required the adoption of modern 3D geometrical photogrammetric survey techniques. These allowed for a very detailed representation of the geometry, which has been adopted in both the 2D limit equilibrium analyses of the slope and in the 3D finite element analyses of the interaction problem. According to this integrated approach, after having accurately reconstructed the three-dimensional geometry, two-dimensional analyses are carried out for selected representative sections, in order to extract information to be then poured in the three-dimensional finite element model. The hydraulic conditions triggering the landslide were not directly measured and 2D limit equilibrium analyses were adopted to back-analyse them as well as studying possible worsening conditions.

The main objective of this study was that of identifying the causes of the detected damages on the structure which, at least in part, were suspected to pre-exist the landslide that, in turn, might have further damaged the structure. This required the analysis of the building and its interaction with the subsoil to be carried out considering first a pre-landslide scenario, to then account for the subsequent landslide event. All the above is here accounted for in the same numerical environment, which allows to consider both the soil and the structure in a realistic 3D coupled non-linear FE model. The landslide had to be first investigated per se: it was back-analysed following a conventional approach, which has highlighted its causes, related to the sudden modifications of the hydraulic conditions occurred just before the failure. The well-understood phenomenon was then reproduced in the coupled FE analyses to finally assess its potential damaging role on the monastery, also considering possible future evolution of the landslide position and extension. The combination of photogrammetric surveys, limit equilibrium analysis and finite element modelling represents, rather than their separate use, one of the main innovative aspects of this research, applied to a complex case-study.

The structure of the paper is as follows: a background on the ancient structure of the Monastery and its historical evolution is first provided, together with the details on the adopted survey techniques and a summary of the back-analysis of the slope failure occurred in 2018. The following Section 3 illustrates the numerical model, providing all the necessary details on the modelled portion of the

structure, the subsoil and the part of the domain reproducing the landslide, the constitutive assumptions and the related calibration of the key mechanical parameters. Section 4 illustrates the sequence of the FE analyses and their main results, while some conclusions are drawn in Section 5.

2. Background

2.1 Santa Scolastica monastery in Subiaco

The structure considered in this study is the Monastery of Santa Scolastica in Subiaco, a picturesque medieval village in the province of Rome close to the Aniene River, in the north-eastern part of the Roman countryside (Figure 1). This area is known for the *Simbruina Stagna*, artificial ponds dating back to the Roman Emperor Nero, created to modify the riverbed around his *villa*, whose ruins are still visible and located close to the road that leads to the Monastery.

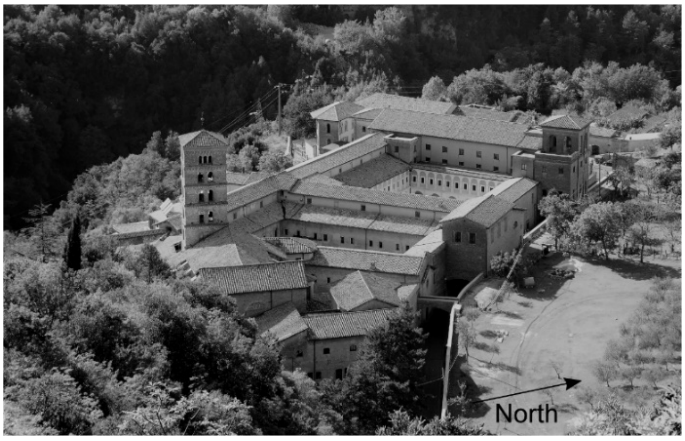

Figure 1: View of the Monastery.

At the end of the V Century, Benedict of Norcia retired to a cave, known as *Sacro Speco*, few kilometres far from the Monastery, its first hermitage, where he founded the Benedictine order.

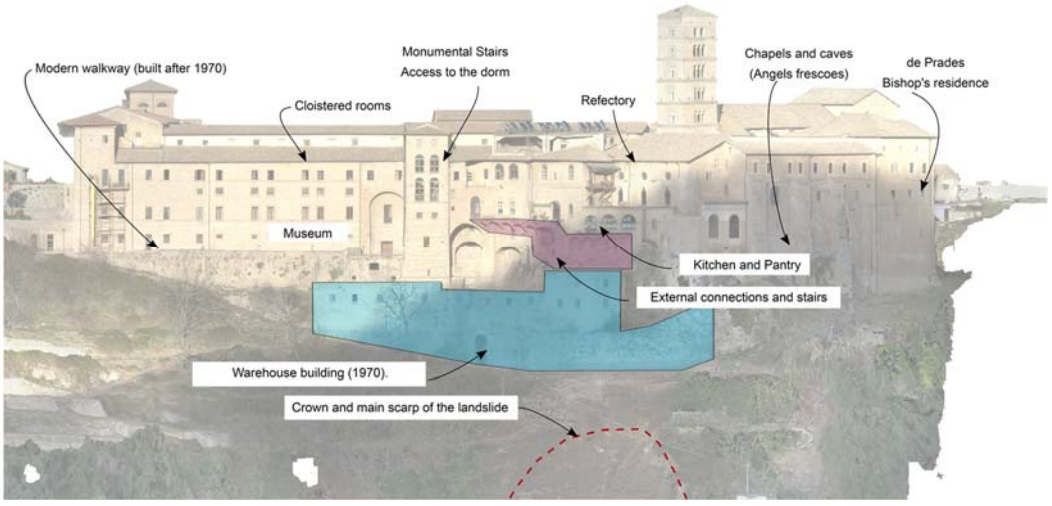

Figure 2: South view of the aggregate.

The Monastery that he dedicated to his sister Scholastica, the first Benedictine nun who died in 543, is the only surviving monastery among the original 13 structures founded in the area by Saint Benedict. The design of the monastery is quite typical. It is enclosed within a wall and the various parts are disposed around the church: the cloisters, the chapter house, refectory and kitchens, the dormitory, the abbot's quarters, the library, the infirmary and the lay brothers' accommodation, storerooms and stables and, in this case, a guest house is also present on the west wing of the aggregate.

Even if the first settlement dates back to the VI-VII Centuries, the structure has undergone deep modifications during time, and its original configuration was only outlined during the Sixties, thanks to the findings of an archaeological campaign (Cerone, 2016).

The most ancient portions of the aggregate are firmly founded on the rock formations and are mainly built with calcareous stones at the lowest levels and with disordered clayey units in the upper and more recent parts. During time and, in particular, during the 20th Century, a number of structural interventions have been made, despite their documentation has mostly been lost or, in some cases, never produced. One of the most significant and recent interventions is the construction of the building highlighted in blue in Figure 2. This building was originally conceived as a warehouse but, soon after its construction (around 1970), some early signs of cracking started to appear on the walls and on the horizontal floor and, consequently, the monks never occupied it. It has been lately found out that the foundations of that building are only partially supported by the rigid rock formation on which the rest of the Monastery has been erected and, as it will be later demonstrated, this condition is responsible for most of the detected structural damage.

Figure 2 shows the southern view of the monastery as obtained from an aerophotogrammetric survey. The most relevant parts of the aggregate are depicted; in particular, the museum and the cloistered rooms where restoration works are currently being realized, the refectory and the *Angels Caves*, constituting the most ancient nucleus of the monastery. In the same figure, some stairs and external passages connecting the kitchens to the warehouse area are highlighted, together with the warehouse building and the crown and the main scarp of the landslide occurred on the 26th of November 2018.

At that time a failure occurred on the south-western slope adjacent to the monastery, causing the interruption of roadway connections and isolating the monks for several days.

This area, however, has experienced a number of landslides in past decades and, during the post-event inspections, evidence of some prevention measures such as gabion walls and retaining nets (presumably installed after another landslide occurred in 2017) was observed. Indeed, these slope

stabilisation actions did not work, as the 2018 failure involved a soil volume including both the nets and the walls.

The cause of the event is to be related to the exceptional rainfalls recorded in that period, which, in combination with an altered vegetation on the slope, triggered the failure conditions. Rainfalls are indeed considered one of the most common causes of natural slope failures (Chen et al., 2004) as the related development of positive pore pressure may produce a significant reduction of soil shear strength.

Due to the vicinity of the crown of the landslide to the structure, possible interaction with the closest parts of the aggregate to the slope needed to be investigated.

2.2 Survey Techniques

Modern surveying technologies allow to capture detailed point clouds outlining the visible geometry of civil engineering structures (*i.e.* external surface profiles and internal ones) with millimetre accuracy. The recording station can be either fixed or installed on a car or a drone, recording millions of georeferenced points moving on pre-designed trajectories. This tool is particularly useful when original drawings are not available or when traditional survey techniques may be inaccurate or too time-consuming. It was successfully adopted to build complex finite element models in the context of seismic assessment of historic masonry structures (Castellazzi, 2017). As reported by recent studies (Giordano, 2019, Clementi, 2020), a detailed geometrical characterization of the structures has a pivotal role in the analysis of complex ancient masonry buildings.

In this study, a complete photogrammetric survey of the exterior of the monastery and of its close surroundings was performed, requiring 8 hours recording. A cloud constituted by approximately 5 million points has then been post-processed and used to determine the shape of the slope failure surface, the geometry of the analysed portion of the structure and the relative position of the building and the landslide crown.

Soil stratigraphy in the area was reconstructed relating the outcrop evidences and the data collected during past surveys in the monastery area, during which two boreholes had been drilled. Nonetheless, mechanical properties of the soil had to be deduced through a back-analysis of the slope, as outlined in the next subsection.

The construction details of the structure were deduced from on-site visual inspections. Due to the advanced degradation state of some rooms the wall section and its typology was visible in some areas where plaster was missing, and some holes had been drilled. Mechanical properties were estimated according to available literature, mainly referring to Italian technical code prescriptions (NTC 2018).

The structural model could undoubtedly benefit from a more accurate experimental campaign on the materials which, unfortunately, was not planned in the context of this study.

2.3 Back Analyses

Back analysis is an effective tool for investigating the strength properties of a soil deposit involved in a landslide. This procedure is adopted to determine the shear strength parameters (c' and ϕ') setting the position of the actual slip surface. In many cases, the topographical profile is more easily determined, while the slip surface is usually determined based on direct (inclinometers) and indirect (morphology-based) observations. In some other cases, the shape of the failure surface is known and some care has to be taken on the determination of the pre-failure geometry.

The limit equilibrium approach is usually adopted in plain-strain two-dimensional (2D) conditions, adopting either simplified (Fellenius (1936), Bishop (1955)) or rigorous methods (Morgenstern & Price, 1965).

This approach allows the identification of the combination of shear strength parameters and hydraulic conditions leading to the occurrence of collapse, expressed by a global safety factor $SF = \tau_f / \tau_{mob} = 1$, where τ_f it the available shear strength along the sliding surface and τ_{mob} is the mobilised shear stress along the same surface.

2.4 FEM analyses for slope stability and interaction problems

The use of numerical methods (finite-element or finite-difference (FD) methods) in structural or geotechnical engineering applications is nowadays common, though their effectiveness strongly depends on geometrical discretisation, initial conditions, correct representation of the construction stages, numerical techniques and constitutive hypotheses (Amorosi, 2014). Less common is the combined use of the approach to couple the response of the soil and the structure in a relatively accurate way, as proposed in this work adopting a non-linear 3D FE modelling procedure.

Nowadays, FE models based on appropriate elasto-plastic constitutive assumptions can be adopted to analyse slope stability problems (Griffiths, 1999), though the use of traditional limit equilibrium methods is often still preferred for its simplicity: this should be related to the objective of the analysis, which in standard engineering practice is limited to the detection of unstable conditions rather than to the prediction of the pre-failure and post-failure displacements, thus not justifying the complexity of a non-linear FE approach in terms of gain of accuracy in the resulting global safety factor *SF*. Conversely, in some other cases, as for example when soil-structure interaction needs to be accounted for, FE models are almost the only solution to get a realistic representation of the phenomena.

FE modelling of landslides entails some specific features, here briefly recalled: no need to assume in advance shape or location of the failure surface if not known a priori, preservation of global equilibrium until *failure* is reached (i.e. up to the step when convergence criteria are satisfied) and availability of results in terms of deformations and displacements. This approach makes it possible to monitor progressive failure, up to and including overall shear failure, relying on the same set of governing data needed in traditional approaches, that is the total unit weight, the shear strength parameters, the geometry of the problem and the distribution of the pore water pressure within the domain (via a piezometric, or water table, height) (Griffiths and Lane, 1999), with the only extra information related to the stiffness of the soil.

In the analyses presented in the following, the landslide has been simulated through strength reduction approach, combined with a variation of the water table height, prescribed on the basis of the back analysis results. In the analyses presented, the non-convergence of the solution (Zienkiewicz & Taylor, 1989) is considered as a suitable indicator of failure. When the algorithm cannot converge within a specified maximum number of iterations, no stress distribution can be found that is simultaneously able to satisfy both the Mohr-Coulomb failure criterion and global equilibrium. Under these conditions, failure is said to have occurred and it is accompanied by a dramatic increase in the nodal displacements within the mesh.

3. Model definition

The three-dimensional FE model has been built based on an accurate description of the geometry of the slope and of the relevant portion of the Monastery, accounting for all the data collected during the surveys and based on the mechanical characterisation of the involved soil and masonry.

3.1 Slope geometry

The area surrounding the Monastery has been inspected through photogrammetric survey and the point-cloud has been post-processed to obtain orthophoto maps, plans, perspective views of the building and of the slope. Being recorded after the event, the point-cloud accurately described the shape of the post-failure geometry of the slope, i.e. its exposed failure surface.

As mentioned above, a key ingredient of any slope stability analysis is the slope geometry in terms of initial configuration and location of the sliding surface. In this case, a reliable representation of these ingredients was possible by selecting a number of vertical sections in the landslide area and in the immediate surroundings, to then superpose the information on the soil profile at different locations.

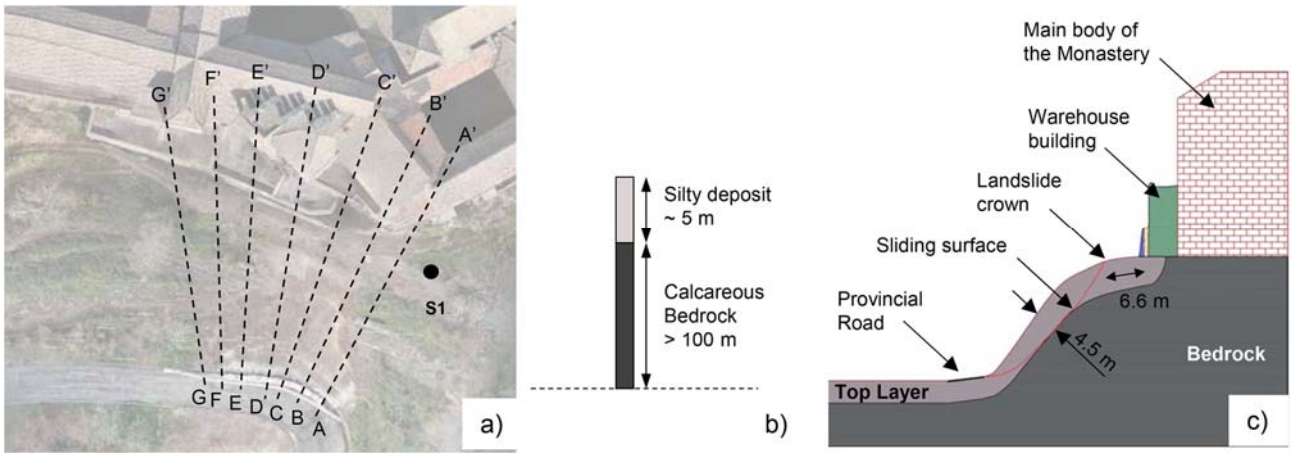

Figure 3: a) Selected vertical sections in plan view, b) S1 available stratigraphy and c) a general section on the slope.

Figure 3c illustrates, by a section, the final model considered representative of the entire slope and adopted to study its stability: it contains all the primary information on the slope, including layer thickness and sliding surface shape.

The aerial view reported in Figure 3a shows the position of the sections, chosen on the basis of the following criteria: sections BB', CC', DD' and EE' cross the scarp and the surface of rupture and have been used to determine the post-failure geometry, sections FF' and GG' lie outside the landslide and have been superposed to the others in order to get information on the intact configuration of the top soil layer. Another section, the AA', is located close to one of the boreholes drilled on site, used to reconstruct the thickness of the two soil layers that characterise the resulting geotechnical subsoil model (Figure 3b): a shallow 5 m thick slightly weakly cemented silty soil stratum laying upon the calcareous bedrock formation.

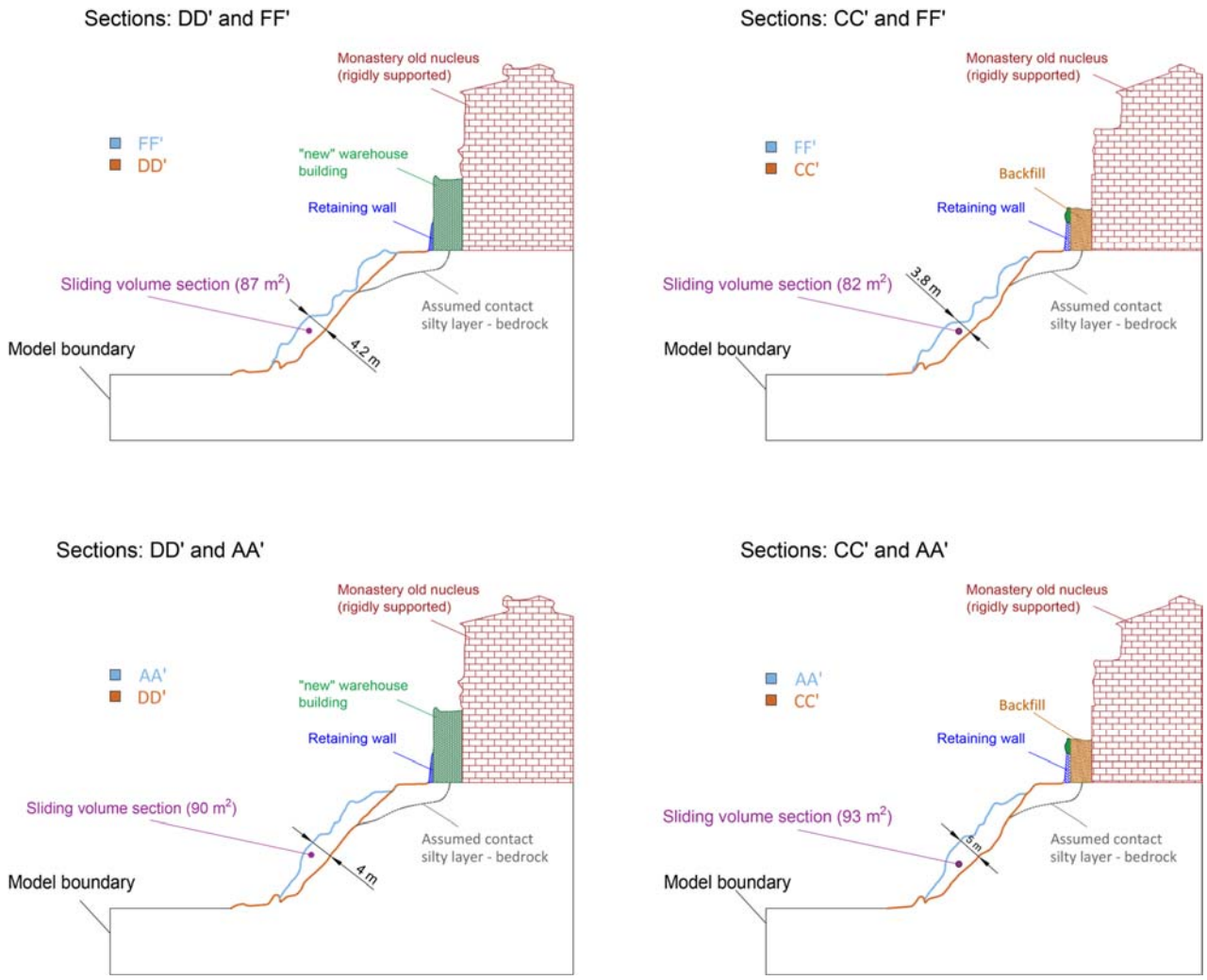

Figure 4: Results of the section superposition.

Section superposition (Figure 4) made it possible to determine the volume of the landslide, calculated as approximately of 2000 m^3. This estimate is in good agreement with the data reported by local authorities soon after the event. Moreover, visual inspection showed that the failure surface is located at the contact between the top soil layer and bedrock, whose outcrop is at an average depth of 4.00 to 5.00 m. In conclusion, the set of information retrieved from the post-processing of the sections consists of distance between the structure and the crown of the landslide (7.0 m), geometry of the landslide, stratigraphy, average slope angles and shape and location of the slip surface. They have all been poured in the bi-dimensional simplified model adopted for the preliminary back analyses.

3.2 Preliminary back analyses

Based on the above discussed geometrical model and the stratigraphy, the back-analyses, performed under plain strain hypothesis adopting the limit equilibrium method proposed by Morgerstern & Price (1965), was aimed at first determining the strength parameters (c' and ϕ') of the

soil layer before the event. For this case-study, the methodology has been also adopted to define the hydraulic conditions that triggered the event and to analyse possible translations/retrogressive movements of the slip surface, calculating for each configuration the safety factor and the triggering conditions in terms of hydraulic head.

The model is characterized by an average slope of the contact between bedrock and clayey layer of 51°, an average ground surface slope equal to 46°. The top silty layer is 4.5 m thick while the height of the slope is equal to 23 m.

In the analyses, the bedrock has been considered as rigid and non-porous, while the top layer is assumed to be characterized by a friction angle equal to 24° and by a unit weight equal to 19 kN/m^3. A uniform distributed load on the top of the slope simulates the presence of the building.

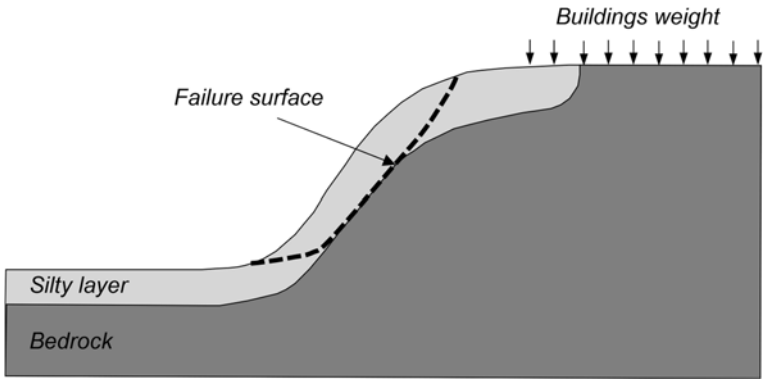

Figure 5: Reference section adopted for the back-analysis.

First, analyses have been performed varying the cohesion c' to mimic the initially stable condition of the slope (SF = 1.15) on the pre-determined failure surface. Based on available observations, absence of pore water pressure was assumed at this stage.

The deduced parameters characterizing the top soil layer are reported in Table 1.

Table 1: Soil parameters.

c'	ϕ'	γ
kPa	°	kN/m^3
25	24	19

The same model has then been adopted to define the triggering transient hydraulic conditions, as induced by the heavy rainfall occurred just before the failure. Hence, referring to the same failure surface, the water table height, measured with reference to the interface between bedrock and top soil

layer (i.e. the failure surface depth) (Figure 6), leading to the decrease of the safety factor to the value of 1.0 was found to be equal to 1.0 m.

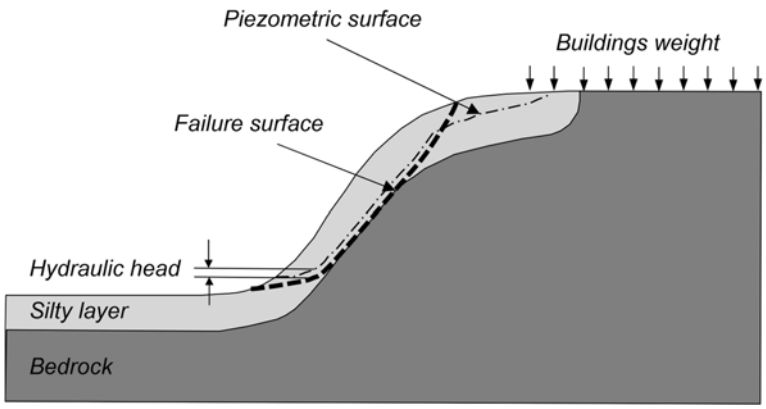

Figure 6: Reference section adopted for the back-analysis and piezometric surface indication.

In order to determine possible future worse conditions on the slope, another section has been analysed, based on the soil profile at GG' (Figure 7). In this case, new failure mechanisms were hypothesized, which could be closer to the building foundations or, in extreme case, under them. The topographic profile (Figure 7b) has been extracted from the point cloud (plan view in Figure 7a), outlining the ground profile of the slope, that in the area is quite regular due to the presence of gabion walls. The stratigraphy of this part has been reconstructed analogously to the previous one. In this case several failure surfaces were hypothesized, determining for each of them the initial factor of safety and the hydraulic conditions sufficient to induce the failure.

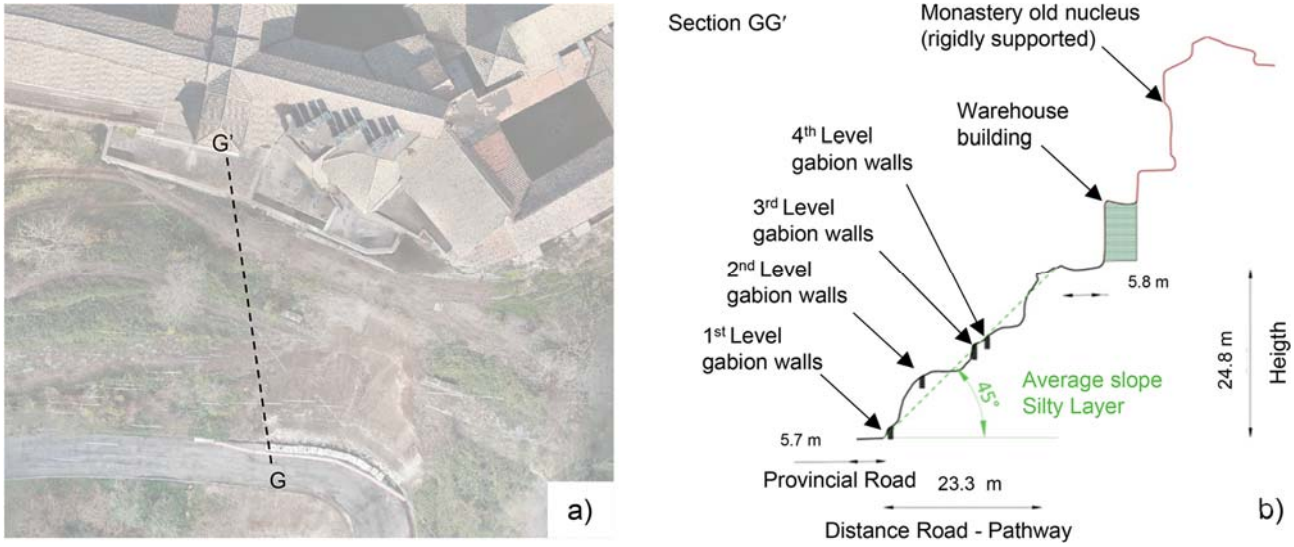

Figure 7: a) Plan view of the additional section out of the landslide footprint and b) detailed description and obtained information.

Among all the analysed failure surfaces, the following three ones are discussed in the following: that for the crown of the failure surface close to the building foundations, the one in which the crown coincides with the most external corner of the foundations and, finally, the failure surface whose crown extends under the building foundations.

Table 2 reports the initial (dry) safety factors corresponding to each of the above mechanisms and the corresponding water table height necessary to trigger the failure.

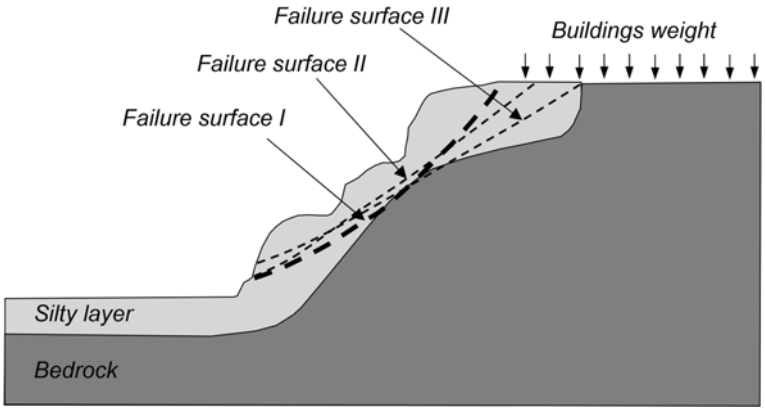

Figure 8: Failure surfaces for the worse-case scenario.

Table 2: Safety factors and water-table heigth on the three selected failure surfaces.

	SF	Water table height to SF = 1
Surface I	1.209	3 m ca.
Surface II	1.340	4 m ca.
Surface III	1.403	4 m ca.

3.3 FEM model: geometry, materials and boundary conditions

The three-dimensional finite element model adopted to study the interaction problem includes the slope and a portion of the monastery, the warehouse building, in which, as mentioned above, most of the damage due to soil-structure interaction phenomena has been located, and that, due to its vicinity to the landslide crown has been judged as the most vulnerable part of the aggregate (Figure 9).

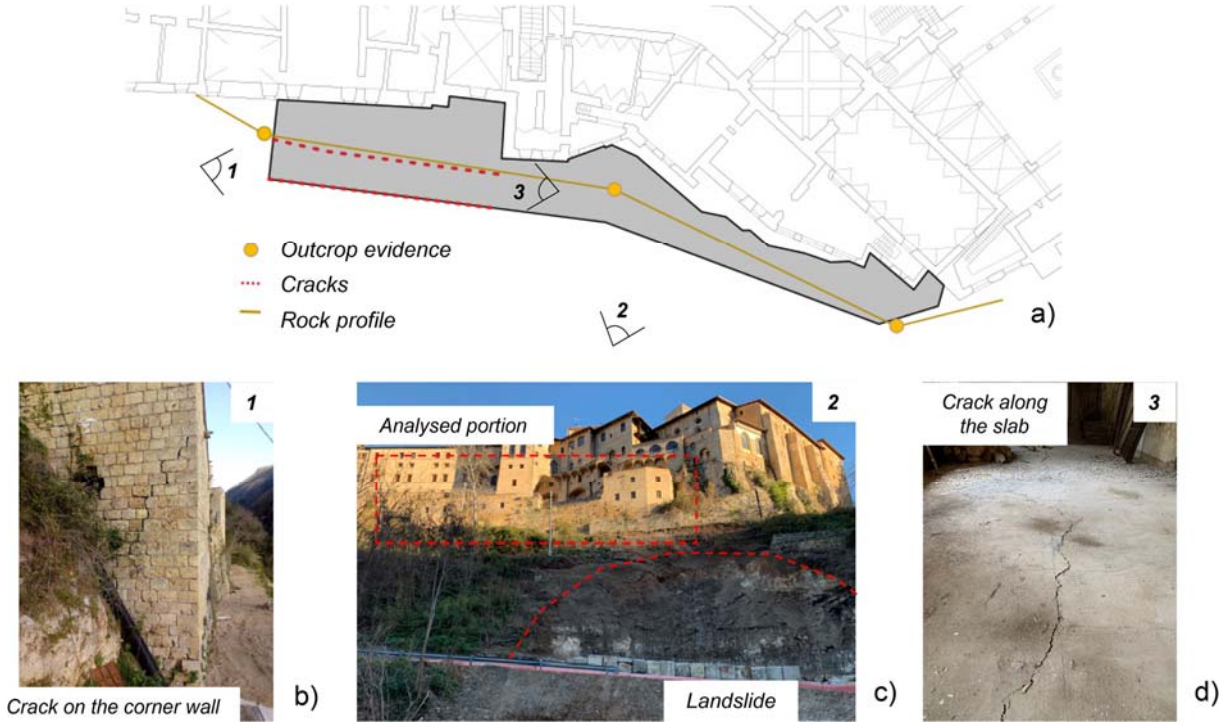

Figure 9: Details on the crack pattern detected and the reconstructed rock profile.

All the necessary details on the soil mechanical parameters, failure surface location and shape were based on the preliminary back-analyses discussed above, while geometry, materials and boundary conditions of the building have been deduced combining visual survey, the information contained in the point-cloud and some data retrieved from historic documentation.

In particular, both the damage in the structure (cracks on the external corner wall and on the slab of the first floor) and the evidences detected on site on the outcropping rock stratum (Figure 9), suggested that part of the structure was not founded on the calcareous bedrock but, instead, on a soil stratum, presumably corresponding to the weakly cemented silty one identified by the available site investigations. This circumstance has been confirmed by the historical reconstruction of the building and by some collected technical information. Moreover, it has been found out that, in order to set a horizontal plane on which the floor could be laid, the rear of the external wall on the southern front was filled with poorly cemented soil up to the first floor height, using at this scope the same silty soil characterising the shallow in-place stratum.

While the most ancient portions of the Monastery were built with calcarenite stones, the modern warehouse has been built with poor rubble stone masonry, with irregular units and, in some cases, with clay brick layers (Figure10). The horizontal structures are realized with reinforced concrete beams and clay bricks, except for the base floor of the warehouse, made of a thin concrete slab. In the model, except for the base floor, horizontal slabs have not been modelled. As in the finite element

model only the front warehouse has been considered, the presence of the Monastery on the back of the structure has been simulated through a rigid block.

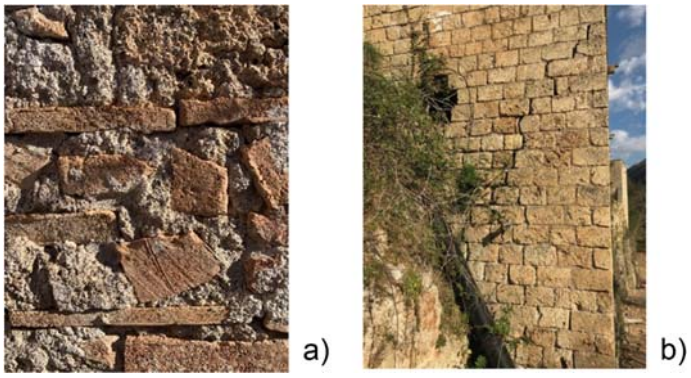

Figure 10: a) Masonry typology in most of the structure, b) western damaged wall and block cover detail.

In all the analyses the contribution of live loads has not been considered, due to the evidence that the structure has never been occupied by anyone. Moreover, to ensure that the overall loading on the foundation was representative of the building, an artificially increased unit weight for the masonry in correspondence of some stripes at the floors levels, to account for the weight of the horizontal elements, has been assumed. In the current analysis, according to literature values for the same masonry typology (NTC2018), the masonry weight was set to 20 kN/m^3, while in the strips it was increased up to 40 kN/m^3.

3.4 Adopted constitutive models

The behaviour of masonry when subjected to ground movements has been investigated resorting to different modelling techniques, i.e. limit analysis (Portioli and Cascini, 2016, 2017), energy-based methods (Iannuzzo et al. 2017) finite element method (Giardina et al. 2013, Franza et al. 2020) and more recently systematic studies on their compared performances have been conducted (Gagliardo et al., 2020, Pepe et al., 2020).

In this paper, in the framework of the finite element method, the constitutive models adopted for the soil and the structure are both formulated according to classic rate-independent plasticity.

The soil behaviour is modelled through a linear elastic-perfectly plastic constitutive model, characterised by a Mohr-Coulomb yield criterion and a null dilatancy angle. This is a relatively simple assumption, but it allows to reproduce the main phenomena involving the soil in the slope movement, while emphasis is given to the effects on the structure in terms of induced damage.

Although a number of failure criteria have been suggested for modelling the strength of soil, the Mohr-Coulomb criterion remains the one most widely used in geotechnical practice (Griffiths and

Lane, 1999). The parameters c' and ϕ' refer to the effective cohesion and friction angle of the soil for which an isotropic behaviour is assumed and defined by E' and ν'.

The constitutive model adopted for the masonry is a three-dimensional anisotropic elastic-perfectly plastic one, based on the Jointed Rock Model, a popular model adopted in rock mechanics. It has been enriched considering block aspect ratio and staggering joints effects to be applicable to periodic block assemblages characterized by an internal structure, such as masonry. The Jointed Masonry Model (Lasciarrea et al., 2019) is characterized by isotropic elasticity: macroscopic elastic properties are derived in the framework of homogenisation theory of periodic media, consisting of a periodic pattern of elastic blocks with cohesive and frictional joints (de Felice et al., 2010) and the equivalent isotropic behaviour is assumed assigning the material an average elastic modulus *E*. Yielding is characterized by the intrinsic material anisotropy: a set of (maximum) three sliding directions, on which failure is meant to occur, is defined in the *xyz* space and described by means of dip (α_1) and strike (α_2). These parameters represent, for each plane, the positive rotation along the *x*-axis and the negative rotation along the *z*-axis, respectively (Sangirardi et al., 2019). In case of masonry panels with regular texture, these angles can be easily defined according to Figure 11.

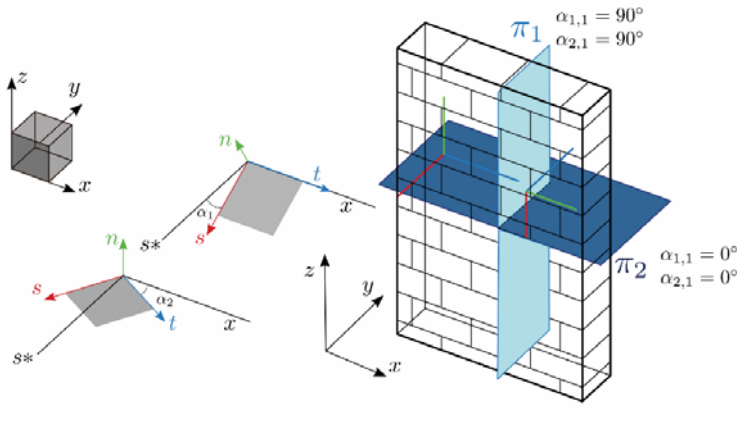

Figure 11: *JMM* bed and head joint plane orientation.

In the analyses here discussed only two planes (head and bed joints) are activated, while a third plane might be considered in case of walls with double facing. Yield functions are defined, for each orientation, in terms of local stress components according to Coulomb's and tensile criterion as follows:

$$f_i^c = |\tau_i| + \sigma_{n,i} \tan\phi_i - c_i \quad (1)$$

$$f_i^t = \sigma_{n,i} - \sigma_{t,i} \quad (2)$$

where i = 1,2,3 is the plane *id*, $\sigma_{n,i}$ and τ_i are the normal and the shear stress along each orientation, ϕ is the friction angle, c_i is the cohesion and $\sigma_{t,i}$ is the tensile strength along the joints. The interlocking effect is accounted by modifying the strength parameters on the head-joints plane, stemming from equilibrium conditions and considering the aspect ratio of the blocks (being b the width of the blocks and a their height) through the parameter β, which also depends on the friction angle of the bed joints:

$$\beta = \tan\phi_2 \frac{b}{2a} \tag{3}$$

Tensile strength and cohesion on the head joints are hence expressed by the following expressions:

$$\sigma_{t,1} = \sigma_{t0,1} - \beta\sigma_{n,2} + c_{0,2}\frac{\beta}{\tan\phi_2} \tag{4}$$

$$c_1 = c_{0,1} - \left(\beta\sigma_{n,2} - c_{0,2}\frac{\beta}{\tan\phi_2}\right)\tan\phi_1 \tag{5}$$

and the modified strength criterion is reported in Figure 3. An associated flow rule has been assumed, but different values of dilatancy ψ_i can, in principle, be defined.

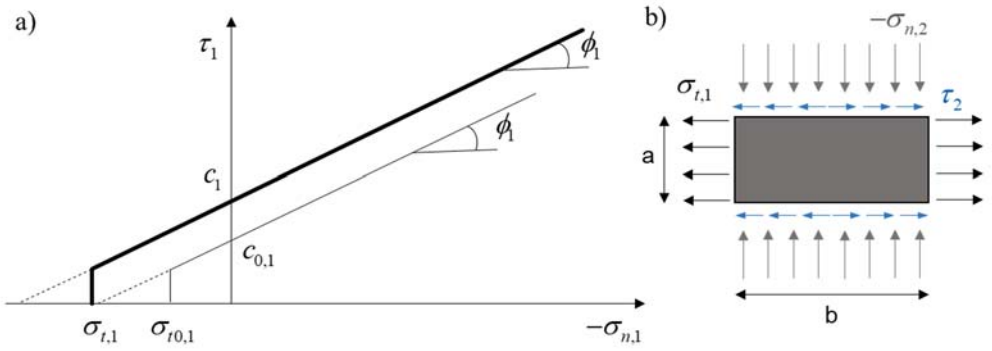

Figure 12: Modified Mohr-Coulomb criterion.

The following tables summarize the adopted mechanical parameters for soil (Table 1) and masonry (Table 2).

Table 3: Soil parameters; Mohr-Coulomb model.

γ	E'	ν'	c'	ϕ'
kN/m^3	MPa		kPa	°
19	50	0.15	25	24

Table 2: Masonry parameters; JMM model.

$c_{0,i}$	$\sigma_{t0,i}$	ϕ_i	β	G	γ
kPa	kPa	°	-	MPa	kN/m^3
20	20	31	0.3	350	20

4. Analyses and Results

The three-dimensional finite element model representing the portion of the monastery on the south front and the surrounding slopes has been built in the software *PLAXIS 3D*. It is formed by 63381 solid 10-noded elements and its footprint is 70×70 m^2. The warehouse building is considered structurally independent from the rest of the aggregate, since it is known that its construction dates back to 1970 and joint-sections are clearly visible in the back side of the building. Nodes at the bottom of the mesh are fixed in both vertical and horizontal directions, while the upper boundary is free in all directions; vertical boundaries are only fixed along the normal direction to the planes.

In Figure 13 a-b two perspective views of a portion of the model show the support conditions of the western side of the building, in which the contact between the side wall and the bedrock is inclined and the most external part is supported by the silty top soil. The south view in Figure 13 b shows the tallest part of the building and the presence of a retaining wall right below it, whose foundations reach the rock formation.

Figure 13 c) shows the building at the first stage of construction. It can be noted that a backfill (characterised by the same properties of the silty soil layer) is present. This detail is in line with some of the information collected on the building process of the structure.

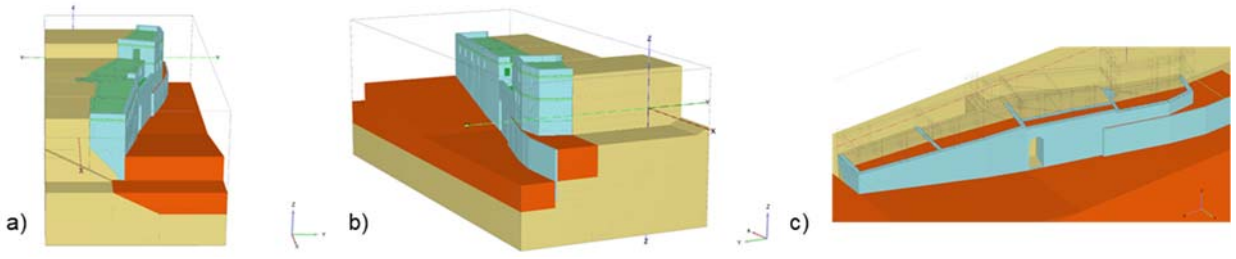

Figure 13: FEM model details: a) western view, b) eastern view and c) construction stage I of the building.

The reproduced scenarios and the analyses performed aimed at first identifying the causes of the pre-landslide existing damage on the structure and then at evaluating possible interaction with the landslide occurred in 2018 in the vicinity of the building in terms of possibly enhanced structural

damage. Finally, new so called *worse-case* scenarios, which might occur in future, are analysed, considering both a translation and a retrogressive evolution of the landslide, as selected based on the preliminary analyses discussed in the previous section.

The results of the numerical simulations are analysed in terms of crack pattern, which is deduced by tensile and shear plastic points, tensile strains and displacements plotted along the most damaged sections. The pre-event configuration, the landslide scenario and the *worse-case* ones are compared with an ideal condition in which the support condition of the building was assumed on rigid foundation, which represents a benchmark case adopted to identify the influence of the soil-structure interaction effects and to highlight the causes of the observed damage.

The calculation sequence consists in the following steps:

1) model initialization (rock and soil volumes are active),
2) structure construction (two different stages reproducing the construction of the two levels of the structure).
3) landslide *activation* : the 2018 landslide scenario is simulated by imposing the critical hydraulic head conditions determined in the preliminary analyses. The *worse-case* scenario is modelled, implementing the effects of the translational and retrogressive evolution of the landslide by considering surface II of Figure 8. It is worth remarking that this scenario is related to extreme and unlikely hydraulic conditions that ought to trigger the sliding (water head at 4.0 m, which, for example, might be compatible with a possible fault of an adjacent water disposal system).

Figure 14 shows the two monitored sections, on which the trend of vertical and horizontal displacements were monitored during the analyses. Section 1, shown in Figure 14a, was placed along the front wall and runs parallel to the horizontal floor on which a longitudinal crack has been observed, while Section 2 (Figure 14b) was placed along the lateral western wall where a marked diagonal crack was detected at the same height of the horizontal slab.

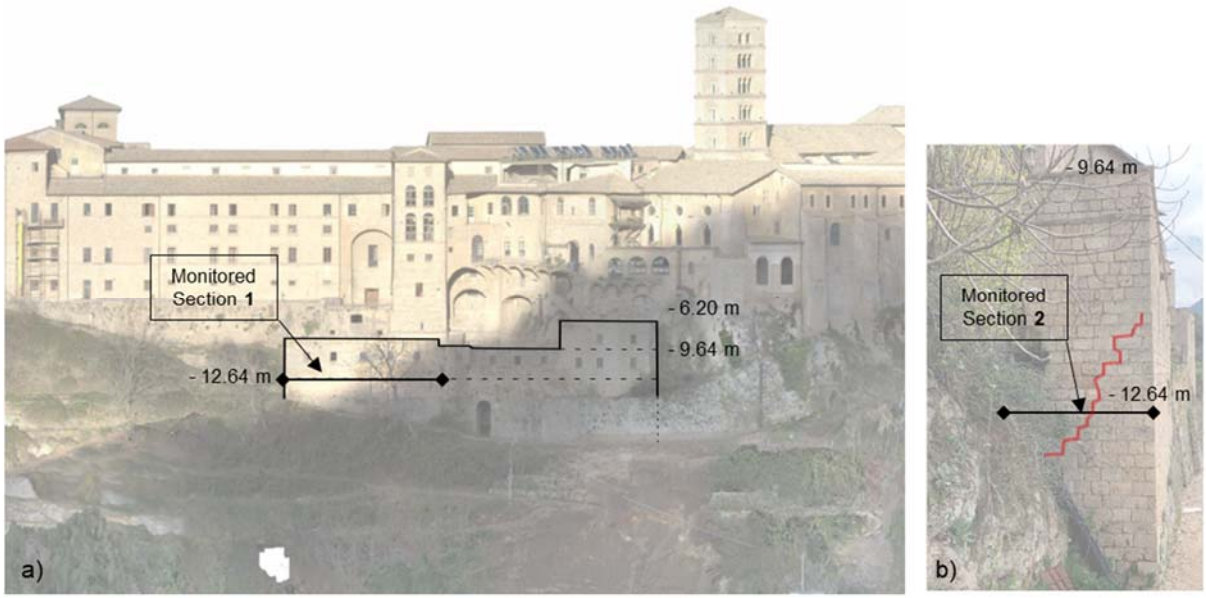

Figure 14: Monitored sections.

The results of the analyses are first illustrated in Figure 15 and 16, where a lateral view of the wall (Figure 15 c) and a top view of the building (Figure 15 a) are reported. Figure 15 d) and e) depict the tensile strain distribution on the horizontal slab of the base floor in the pre-event and in the worse case scenario respectively. In Figure 16 the plastic points (blue points indicate shear failure while brown ones indicate tensile failure) on the wall are plotted, in order to represent its damage pattern in the analysed conditions.

Figure 16 shows for the pre-event stage a concentration of plastic points on the western wall, mostly related to shear failure, consistently with the diagonal crack observed at that location during the survey. At the same post-construction stage of the analysis (Figure 15 d and e), tensile strains predicted by the numerical model concentrates along the horizontal floor with a geometrical pattern very similar to the observed one on the real structure. This results clearly indicate that, already at the pre-landslide stage, the structure had cumulated significant damage, which was triggered by the differential settlements related to the heterogeneous foundation soil: in fact, the rear of the warehouse building lays on the stiff calcareous rock, while the front interacts with the softer silty soil. This feature is very well reproduced by the numerical model, as it realistically accounts for the non-linear soil-structure interaction processes.

To highlight the role of the subsequent landslides, the above results are compared to the ones resulting for the simulations of the November 2018 landslide and the final, more extreme, landsliding scenario. Figure 16 indicates that the plastic points distribution along the lateral wall is only barely modified by both landslide events, which, at the same time, do not induce any sensitive variations of the tensile strains resulting on the horizontal slab.

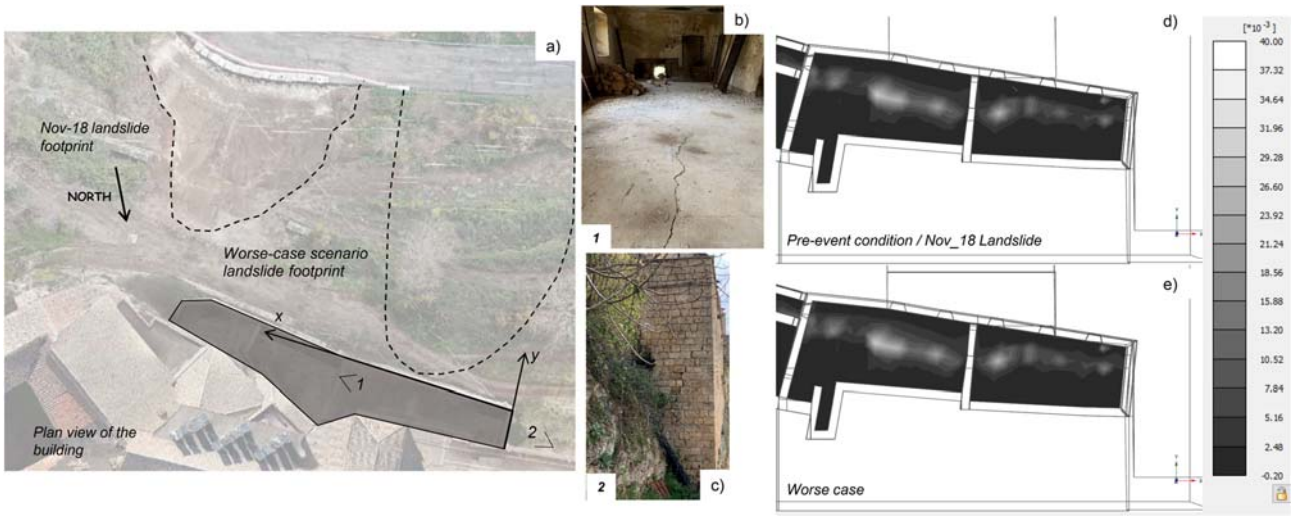

Figure 15: a) Top view of the structure and localization of the modelled landslides, b) crack on the horizontal slab of the base floor, c) crack on the western wall, tensile strain distribution in the pre-event d) and landslide e) scenarios.

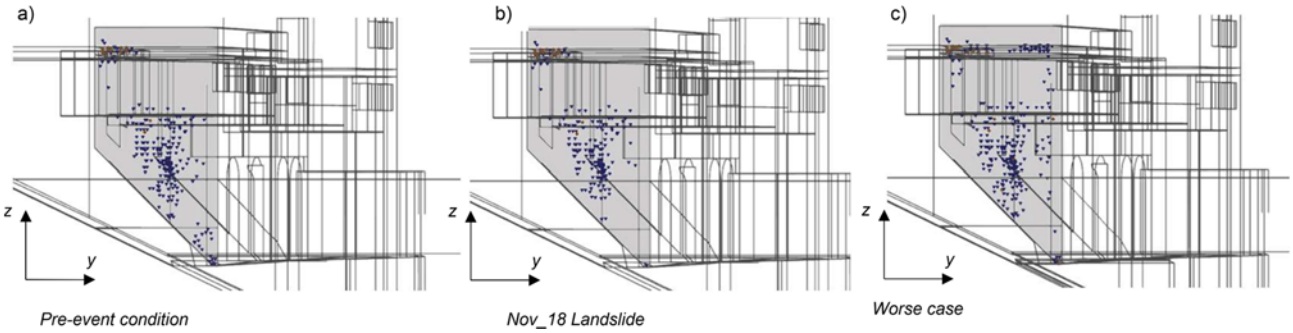

Figure 16: Crack pattern in the pre event a), after the occurred landslide b) and in the worse-case scenario c).

Figure 17 b) and c) report the out-of-plane (u_y) and the vertical displacement (u_z) respectively, as obtained along the Section 1 highlighted in bold in Figure 17a). Both the out-of-plane and the vertical displacements do not seem to be influenced by the real landslide condition, while an overall increase can be observed in the worse-case scenario.

The solid black line, outlining the correspondent quantities in the ideal case of rigidly supported foundations, shows that, albeit negligible, out-of-plane displacements can still be envisaged as well as the corresponding, slightly larger, vertical ones: the first can be explained by the presence of the backfill, thrusting on the wall and causing the shape that characterizes the distribution also in the other three cases. The localized decrease is related to the presence of a thick transverse wall. For the same case of rigid foundation, the vertical displacement is instead related to the masonry deformability, while in case of heterogeneous soil foundation the trend in the pre- and post-event

conditions seem to coincide. Higher values are, as expected, recorded in the worse case scenario, in which the crown of the landslide extends right below the monitored wall.

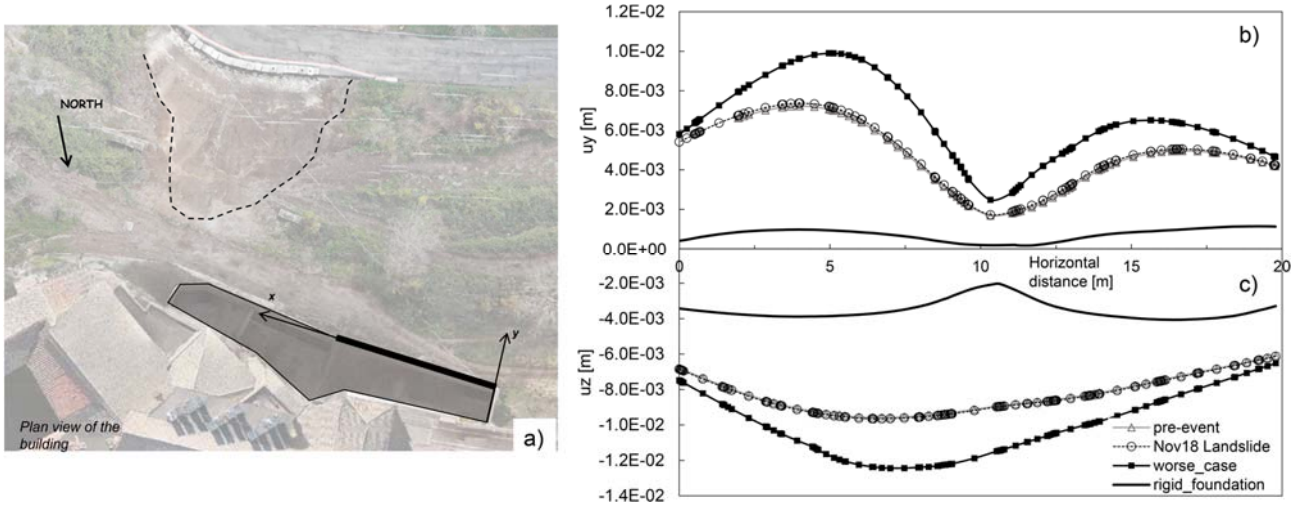

Figure 17: Horizontal (b) and vertical (c) displacement on Section 1 (a) in the four scenarios.

Figures 18 b) and c) report the horizontal and vertical displacement along the lateral Section 2 (Figure 18a), highlighted in bold black line in same figures. This section runs parallel to the floor on the western damaged wall and, in case of rigid foundations, both the vertical and the horizontal displacements exhibit a response driven by the masonry deformability and the sole contribution of the backfill on the transverse wall, respectively.

The results plotted for the other three scenarios indicate a considerable increase around points located at 2.5 - 3.0 m on the abscissa, which coincides with the location of the crack on the horizontal slab and with the interface between rock and backfill.

The magnitude of the displacements obtained by the numerical analysis is comparable with that observed on site and compatible with the existing crack pattern on the structure.

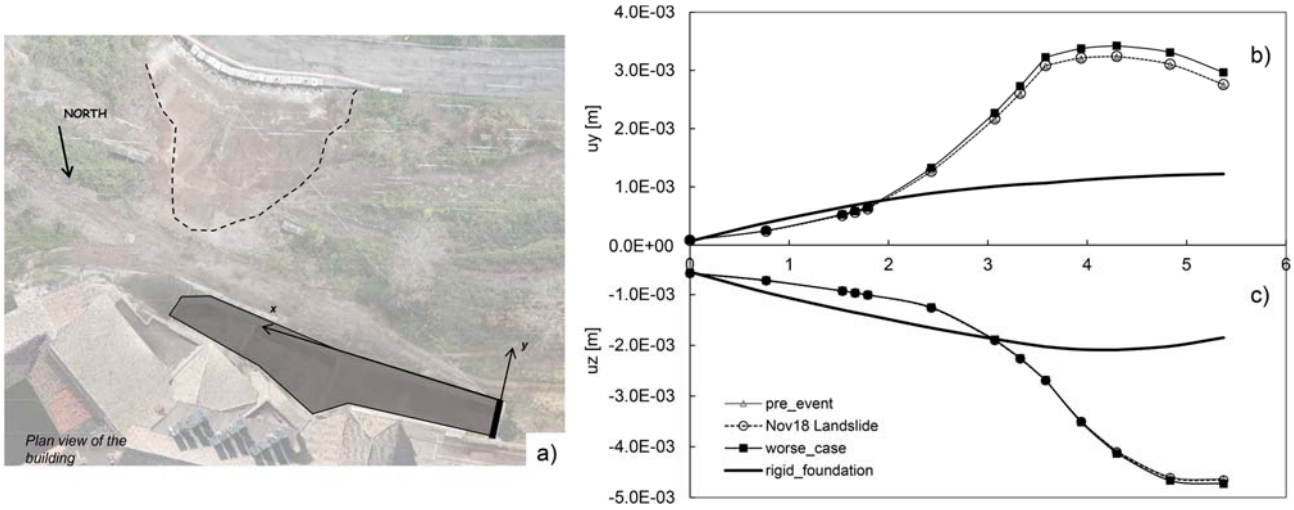

Figure 18: Horizontal (b) and vertical (c) displacement on Section 2 (a) in the four scenarios.

5. Conclusions

The area in which the Monastery of Santa Scolastica was founded by Benedict of Norcia is particularly prone to landslides. Nonetheless, no evident sign of damage clearly related to slope movements had historically been reported with reference to the oldest nucleus of the Monastery.

However, in November 2018 a landslide occurred in the vicinity of the most modern part of the building, on the southern front of the aggregate. During post-event surveys a harmful damage pattern was detected on this portion of the building and both its origin and a possible evolution related to the slope movement had to be determined.

At the scope, three-dimensional numerical analyses were performed, accounting for the complex geometrical features of both the building and the slope, which were surveyed through modern and semi-automatic tools. Decisive information came from the reconstruction of the rock profile, which highlighted that the foundations of the building were only partly supported by this rigid formation, as also interacting with a softer soil stratum.

The coupled structural and geotechnical numerical analyses were performed assuming different scenarios, in order to reproduce the pre- and post- event conditions. Moreover, two ideal cases were also considered, namely simulating an improvement of the support conditions of the building, in which the foundations are assumed to be rigidly supported by the bedrock, and a worse case in which the landslide involves a soil volume closer to the construction, for which the triggering hydraulic conditions have been preliminarily determined.

The results offered a useful insight into the safety conditions of the construction and allowed to track back the origin of the observed damage to construction details, excluding that the landslide event occurred in 2018 had worsened the already compromised pre-existing condition. Extreme conditions were also evaluated shading some light into the detection of possible future sources of damage. The results of the analysis of the ideal case of rigid support on the one hand were used to determine that the cause of the observed crack pattern had to be identified in the foundation support, while proving that damage connected to foundation settlements can be reasonably excluded on the rest of the monastery, being almost entirely built on the calcarenite formation. This represent a concrete help for the evaluation of the safety of the entire structure and, at the same time, a valuable technical lesson learned from the past.

6. Acknowledgments

This work was supported by the Regione Lazio (SiCura 2018-2020) Research Grant and by the DPC/ReLUIS 2019-2021 Research Project. The Author wish to thank also the Polo Museale del Lazio (Museum Center of Lazio) of the Italian Ministry of Cultural Heritage.

7. References

Amorosi, A., Boldini, D., de Felice, G., Malena, M. and Sebastianelli, M., 2014. Tunnelling-induced deformation and damage on historical masonry structures. *Géotechnique*, *64*(2), pp.118-130.

Bishop, A.W., 1955. The use of the slip circle in the stability analysis of slopes. *Géotechnique*, *5*(1), pp.7-17.

Canuti, P., Margottini, C., Fanti, R. and Bromhead, E.N., 2009. Cultural heritage and landslides: research for risk prevention and conservation. In *Landslides–disaster risk reduction* (pp. 401-433). Springer, Berlin, Heidelberg.

Castellazzi, G., D'Altri, A.M., de Miranda, S. and Ubertini, F., 2017. An innovative numerical modeling strategy for the structural analysis of historical monumental buildings. *Engineering Structures*, *132*, pp.229-248.

Cerone, R., 2016. *La regola e il monastero: arte e architettura in Santa Scolastica a Subiaco (secc. VI-XV)*. Campisano editore.

Chen, H., Lee, C.F. and Law, K.T., 2004. Causative mechanisms of rainfall-induced fill slope failures. *Journal of geotechnical and geoenvironmental engineering*, *130*(6), pp.593-602.

Clementi, F., Milani, G., Ferrante, A., Valente, M. and Lenci, S., 2020. Crumbling of Amatrice clock tower during 2016 Central Italy seismic sequence: Advanced numerical insights. *Frattura ed Integrità Strutturale*, *14*(51), pp.313-335.

Giordano, E., Clementi, F., Nespeca, A. and Lenci, S., 2019. Damage assessment by numerical modeling of sant'agostino's sanctuary in offida during the central italy 2016–2017 Seismic Sequence. *Frontiers in Built Environment*, *4*, p.87.

Cruden, D.M. and Varnes, D.J., 1996. Landslides: investigation and mitigation. Chapter 3-Landslide types and processes. *Transportation research board special report*, (247).

de Felice, G., Amorosi, A. and Malena, M., 2010. Elasto-plastic analysis of block structures through a homogenization method. *International journal for numerical and analytical methods in geomechanics*, *34*(3), pp.221-247.

Del Soldato, M., Di Martire, D., Bianchini, S., Tomás, R., De Vita, P., Ramondini, M., Casagli, N. and Calcaterra, D., 2019. Assessment of landslide-induced damage to structures: the Agnone

landslide case study (southern Italy). *Bulletin of Engineering Geology and the Environment*, *78*(4), pp.2387-2408.

Fellenius, W., 1936. Calculation of stability of earth dam. In *Transactions. 2nd Congress Large Dams, Washington, DC, 1936* (Vol. 4, pp. 445-462).

Ferlisi, S., Nicodemo, G., Peduto, D., Negulescu, C. and Grandjean, G., 2019. Deterministic and probabilistic analyses of the 3D response of masonry buildings to imposed settlement troughs. *Georisk: Assessment and Management of Risk for Engineered Systems and Geohazards*, pp.1-20.

Franza, A., Acikgoz, S. and DeJong, M.J., 2020. Timoshenko beam models for the coupled analysis of building response to tunnelling. *Tunnelling and Underground Space Technology*, *96*, p.103160.

Gagliardo, R., Cascini, L., Portioli, F., Landolfo, R., Tomaselli, G., Malena, M. and de Felice, G., 2020. Rigid block and finite element analysis of settlement-induced failure mechanisms in historic masonry wall panels. *Frattura ed Integrità Strutturale*, *14*(51), pp.517-533.

Giardina, G., Van de Graaf, A.V., Hendriks, M.A., Rots, J.G. and Marini, A., 2013. Numerical analysis of a masonry façade subject to tunnelling-induced settlements. *Engineering structures*, *54*, pp.234-247.

Griffiths, D.V. and Lane, P.A., 1999. Slope stability analysis by finite elements. *Geotechnique*, *49*(3), pp.387-403.

Iannuzzo, A., Angelillo, M., De Chiara, E., De Guglielmo, F., De Serio, F., Ribera, F. and Gesualdo, A., 2018. Modelling the cracks produced by settlements in masonry structures. *Meccanica*, *53*(7), pp.1857-1873.

ISPRA. Landslides in Italy. Special Report 2008; ISPRA: Roma, Italy, 2008; ISBN 978-88-448-0355-1.

Lasciarrea, W.G., Amorosi, A., Boldini, D., de Felice, G. and Malena, M., 2019. Jointed Masonry Model: A constitutive law for 3D soil-structure interaction analysis. *Engineering Structures*, *201*, p.109803.

Mavrouli, O., Fotopoulou, S., Pitilakis, K., Zuccaro, G., Corominas, J., Santo, A., Cacace, F., De Gregorio, D., Di Crescenzo, G., Foerster, E. and Ulrich, T., 2014. Vulnerability assessment for reinforced concrete buildings exposed to landslides. *Bulletin of engineering geology and the environment*, *73*(2), pp.265-289.

Mavrouli, O., Giannopoulos, P.G., Carbonell, J.M. and Syrmakezis, C., 2017. Damage analysis of masonry structures subjected to rockfalls. *Landslides*, *14*(3), pp.891-904.

Morgestern N.R., Price V.E. 1965. The analysis of the stability of generalised slip surfaces. *Géotechnique*, *15*, pp.79-93.

Negulescu, C., Ulrich, T., Baills, A. and Seyedi, D.M., 2014. Fragility curves for masonry structures submitted to permanent ground displacements and earthquakes. *Natural hazards*, *74*(3), pp.1461-1474.

Palmisano, F. and Elia, A., 2014. Behaviour of masonry buildings subjected to landslide-induced settlements. *International Journal of Structural Engineering*, *5*(2), pp.93-114.

Palmisano, F. and Elia, A., 2015. Shape optimization of strut-and-tie models in masonry buildings subjected to landslide-induced settlements. *Engineering Structures*, *84*, pp.223-232.

Palmisano, F., Vitone, C. and Cotecchia, F., 2018. Assessment of landslide damage to buildings at the urban scale. *Journal of Performance of Constructed Facilities*, *32*(4), p.04018055.

Parisi, F., Galasso, C. and Sabella, G., 2015. Fragility of reinforced concrete framed structures to flow-type landslides. In *12th International Conference on Applications of Statistics and Probability in Civil Engineering (ICASP12)*.

Parisi, F. and Sabella, G., 2017. Flow-type landslide fragility of reinforced concrete framed buildings. *Engineering Structures*, *131*, pp.28-43.

Peduto, D., Nicodemo, G., Caraffa, M. and Gullà, G., 2018. Quantitative analysis of consequences to masonry buildings interacting with slow-moving landslide mechanisms: a case study. *Landslides*, *15*(10), pp.2017-2030.

Pepe, M., Sangirardi, M., Reccia, E., Pingaro, M., Trovalusci, P. and de Felice, G., 2020. Discrete and Continuous Approaches for the Failure Analysis of Masonry Structures Subjected to Settlements. *Frontiers in Built Environment*, *6*, p.43.

Portioli, F. and Cascini, L., 2016. Assessment of masonry structures subjected to foundation settlements using rigid block limit analysis. *Engineering Structures*, *113*, pp.347-361.

Portioli, F. and Cascini, L., 2017. Large displacement analysis of dry-jointed masonry structures subjected to settlements using rigid block modelling. *Engineering Structures*, *148*, pp.485-496.

Puzrin, A.M., Alonso, E.E. and Pinyol, N.M., 2010. *Geomechanics of failures*. Springer Science & Business Media.

Sangirardi, M., Malena, M. and de Felice, G., 2019, September. Settlement Induced Crack Pattern Prediction Through the Jointed Masonry Model. In *Conference of the Italian Association of Theoretical and Applied Mechanics* (pp. 1971-1980). Springer, Cham.

Zienkiewicz, O.C., Taylor, R.L., Nithiarasu, P. and Zhu, J.Z., 1989. *The finite element method* (Vol. 1). London: McGraw-hill.